Journal of Magnetics 9(3), 69-74 (2004)

Noise Reduction of Geomagnetic Signals From Randomly Oriented Sensors

Yong J. Song[1]*, Choong S. Lee[1], Ki C. Kim[2], Sun-Ho Lim[3], Duk-Yung Kim[3], Dong-Hwan Son[4] and Dae Y. Kim[4]

[1]*Department of Physics, Ajou University, Wonchon-dong Youngtong-gu, Suwon 443-749, Korea*
[2]*Electronics and Telecommunications Research Institute, 161 Gajeong-dong Yuseong-gu, Daejeon 303-305, Korea*
[3]*LG Innotek Co., Ltd. 148-1 Mabuk-Ri Gusung-Myun, Yongin 449-910, Korea*
[4]*Naval Weapon Systems R&D Center, P.O. Box 18, ChinHae 645-600, Korea*

(Received 17 April 2004)

A method of processing signals of unaligned geomagnetic sensors placed on the seabed is presented. The offset drifts of the fluxgate sensors are processed by polynomial fitting and the orientations of the sensor axes are found by minimizing the noise power using wavelet analysis. The noise power was reduced by 9.1 dB by processing the components of magnetic field separately using subtraction filter, polynomial fitting and wavelet analysis.

Key words : geomagnetic signal, noise reduction, subtraction filter, fluxgate sensor

1. Introduction

Magnetic signal from a moving ship ranges from 0.1 nT to 100 nT depending on the size of the ship and the distance from the sensor. For the detection of a moving vessel, it is important to reduce the noise of the geomagnetic field, which varies up to 100 nT daily and contains low frequency components in the range of 1 mHz to 1 Hz in which the target signal also lies.

It was reported that a good coherence exists between geomagnetic signals of two sensors within as much as 1 mile distance for a frequency range from 0 to 20 MHz [1]. Therefore common geomagnetic noises can be removed by preprocessing the signals with subtraction filtering, where the signal from the detection sensor is subtracted by that from a reference sensor [2]. Most of the previous researches were done with aligned sensors. However, it is hard to align the axes of a sensor in a sensor array installed on a sea bottom.

In this research, three sensors at distances of about 100 m between them were placed on a sea bed about 50 m under the sea surface. Three-axis fluxgate sensors were used and their axes were not aligned. The fluxgate sensors usually show offset drifts which sometimes amount to an order of ten nT a day. The difficulties of preprocessing the signals with offset drifts without knowing the axis directions will be discussed and a way of finding the orientations of the sensor axes will be presented.

*Corresponding author: Tel: +82-31-219-2574, e-mail: yjsong@ajou.ac.kr

2. Theory

2.1. Subtraction Filter

Fig. 1 shows how to remove the daily change of the geomagnetic field by using subtraction filter. In processing signals from a sensor, another sensor within a distance of good coherence for the geomagnetic field is chosen as a reference. Equation (1) shows the way of preprocessing the signals using subtraction filter under the assumption that the axes of the sensors have been aligned,

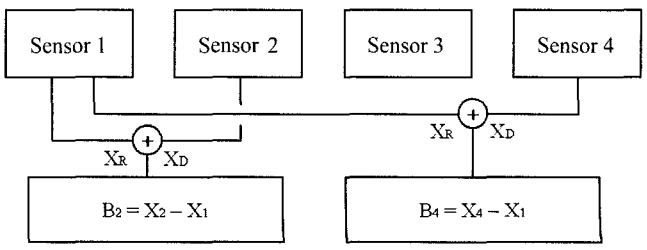

Fig. 1. Selection of a detection sensor and a reference sensor in a sensor array.

$$\boldsymbol{B} = \boldsymbol{B}_d - \boldsymbol{B}_r \tag{1}$$

where $\boldsymbol{B}_d$ and $\boldsymbol{B}_r$ are the signals from the detection sensor and reference sensor, respectively. Because of the vector nature of the magnetic field, there exist three signals corresponding to the three axes of the sensors and the good coherence of the signals applies only to the same components of the magnetic fields. If the sensor axes are not aligned, we can think of a method of applying the subtraction filter to the magnitude of the signal vectors as described in the following equation:

$$\begin{aligned} B &= B_d - B_r \\ &= \sqrt{B_{dx}^2 + B_{dy}^2 + B_{dz}^2} - \sqrt{B_{rx}^2 + B_{ry}^2 + B_{rz}^2} \end{aligned} \tag{2}$$

As mentioned above, signals from the fluxgate sensors have offset drifts which may accumulate up to an order of 10 nT as time goes on. Let $\boldsymbol{R}$ be the offset drift of a sensor, and $\boldsymbol{b}$ be the observed geomagnetic field. The output signal of a sensor can be written as the following equation:

$$\boldsymbol{B} = \boldsymbol{R} + \boldsymbol{b} \tag{3}$$

$\boldsymbol{R}$ in equation (3) has a random direction. If one is interested only in short time changes so that $\boldsymbol{R}$ and $\boldsymbol{b}$ denote the changes from those at a fixed time, and if $|\boldsymbol{R}| >> |\boldsymbol{b}|$,

$$\begin{aligned} B &= \sqrt{\boldsymbol{B} \cdot \boldsymbol{B}} = \sqrt{R^2 + 2R \cdot b + b^2} \\ &\approx R + \frac{\boldsymbol{R}}{R} \cdot \boldsymbol{b} \end{aligned} \tag{4}$$

where $(\boldsymbol{R}/R)\ \boldsymbol{b}=b_{\mathrm{R}}$ is the component of $\boldsymbol{b}$ in the direction of $\boldsymbol{R}$ and we can only observe $R+b_R$. Applying subtraction filter to the signals from two sensors, S_1 and S_2, the result will be

$$\begin{aligned} B_{21} &= B_2 - R_1 \\ &= (R_2 - R_1) + (b_{R2} - b_{R1}) \end{aligned} \tag{5}$$

The term $(R_2 - R_1)$ is a slowly varying function of time and can be removed by a polynomial fitting. However, $\boldsymbol{R}_2$ and $\boldsymbol{R}_1$ are vectors with random directions so we cannot expect a good coherence between b_{R2} and b_{R1} and $(b_{R2} - b_{R1})$ will still be a source of large noise.

When there is a target signal, $\boldsymbol{b}$ in equation (3) can be redefined as $\boldsymbol{b} = \boldsymbol{b}_{gm} + \boldsymbol{b}_t$ where $\boldsymbol{b}_{gm}$ and $\boldsymbol{b}_t$ are geomagnetic noise and target signal, respectively. Under the condition of equation (4), only the projection of $\boldsymbol{b}_t$ on $\boldsymbol{R}$ will be observed rather than its absolute value. Therefore, this method may reduce the target signal in an unexpected way.

2.2. Finding the axis orientations

2.2.1 Rotation of axes

The discussions above indicates that the subtraction filter should be applied only to parallel components of detection and reference signals and that we have to find the axis orientations of the sensors. If we find the directions of axes of a detection sensor with respect to the coordinate axes of the reference sensor, we can rotate coordinate axes of the reference sensor and get the components of magnetic field parallel to the detection sensor axes.

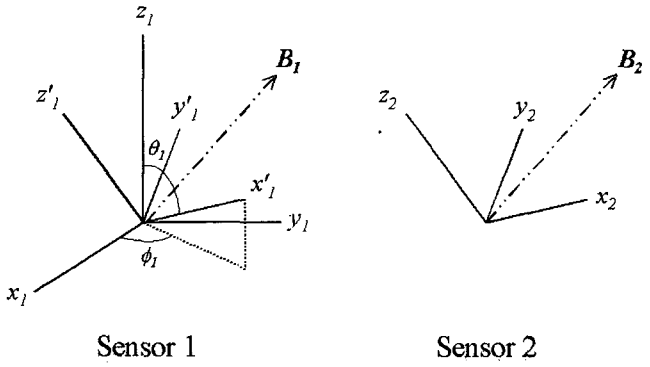

Fig. 2. Transformation between the two coordinate systems corresponding to two sensors.

In Fig. 2, the axes x_1, y_1, and z_1 of sensor 1 and x_2, y_2, and z_2 of sensor 2 are shown. Sensor 2 will be considered as the detection sensor. $\boldsymbol{B}_1$ and $\boldsymbol{B}_2$ are the magnetic fields measured at the same time. If we remove high frequency parts from the signals, $\boldsymbol{B}_1$ and $\boldsymbol{B}_2$ will represent only low frequency parts and they will be the same vectors. The axes x'_1, y'_1, and z'_1 in Fig. 2 represent the rotated coordinate axes which are expected to be parallel to the corresponding axes of sensor 2.

The components of $\boldsymbol{B}_1$ in this rotated coordinates can be obtained by the following equation:

$$\begin{pmatrix} B'_{1x} \\ B'_{1y} \\ B'_{1z} \end{pmatrix} = \begin{pmatrix} a_{11} & a_{12} & a_{13} \\ a_{21} & a_{22} & a_{23} \\ a_{31} & a_{32} & a_{33} \end{pmatrix} \begin{pmatrix} B_{1x} \\ B_{1y} \\ B_{1z} \end{pmatrix} \tag{6}$$

If we specify the direction of x'_1, y'_1, and z'_1 axes in the unprimed coordinate system by (θ_1, ϕ_1), (θ_2, ϕ_2), etc. in the spherical polar coordinates, the elements in the first row of rotation matrix are

$$a_{11} = \sin\theta_1 \cos\phi_1,\ a_{12} = \sin\theta_1 \sin\phi_1,\ a_{13} = \cos\theta_1 \tag{7}$$

Therefore, preprocessing the signal B_{2x} of sensor 2 with subtraction filter will be

$$B_{21x} = B_{2x} - B'_{1x} \tag{8}$$

where $B'_{1x} = a_{11}B_{1x} + a_{12}B_{1y} + a_{13}B_{1z}$ with sensor 1 taken as the reference.

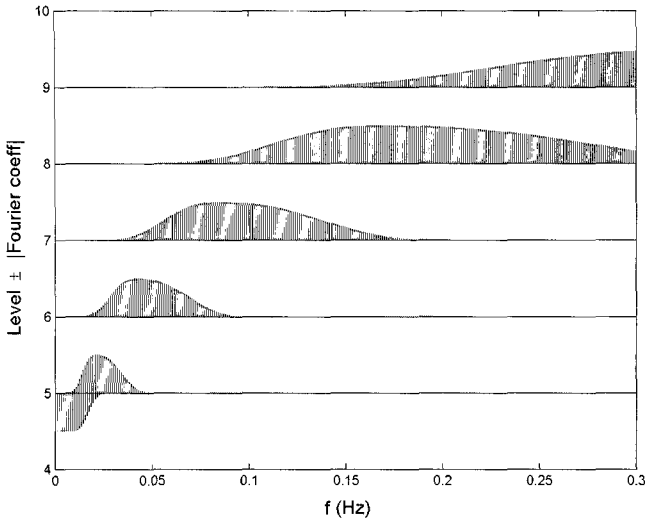

Fig. 3. Bar graphs of absolute values of Fourier coefficients of Symmlet8 with n = 1024. Bars for level 5 scaling function are plotted underneath the level line while bars for wavelets are plotted over the level line.

2.2.2. Discrete Wavelet Transformation

Discrete measurement data with total number $n = 2^{J_1}$ can be expanded with scaling functions and wavelets as follows:

$$f(t) = \sum_{k=0}^{n_{J_0}-1} c_{J_0,k}\phi_{J_0,k}(t) + \sum_{J=J_0}^{J_1-1}\sum_{k=0}^{n_J-1} d_{J,k}\Psi_{J,k}(t) \qquad (9)$$

where $\Psi_{J,k}(t)$'s are wavelets and $\phi_{J_0,k}(t)$'s are scaling functions. For each level J, the number of wavelets or scaling functions is $n^J = 2^J$. In this research, Symmlet8 was used with $J_0 = 5$ and $J_1 = 10$ with $n = 1024$.

The frequency range of the scaling functions and wavelets of Symmlet8 are shown in Fig. 3. As the level number gets higher, the frequency range of wavelets gets higher and broader and it is expected that the coherence between detection and reference signals gets lower.

2.2.3. Algorithm

As discussed in section 2.2.1, we can find the direction of x_2-axis of sensor 2 by minimizing the noise of B_{21x} in equation (8). If x_1' axis is not parallel to x_2 axis in Fig. 2, the noise in B_{21x} in equation (8) will be larger. Therefore, we can select (θ_1, ϕ_1) as parameters in minimizing the rms noise of B_{21x}.

The first step is to calculate B_{21x} with arbitrary starting angles of (θ_1^i, ϕ_1^i). The second step is to perform a polynomial fitting since offset drifts of sensor 1 and 2 still exist and are superposed in B_{21x}. The next step is to perform wavelet transformation and inverse transformation to remove higher frequency parts of the signal to get the best coherence of the two sets of data. Finally, the rms noise is calculated and the above process is repeated to find the best set of angles (θ_1, ϕ_1) which minimizes the rms noise.

In the above process, the data in the time ranges which include target signals such as those from ships should be removed. For this purpose, the data may be divided into windows with fixed number of data points and the windows without any target signal should only be used. The procedure is summarized in the following :

1) Calculate $B_{21x} = B_{2x} - B_{1x}'$ for windows with 600 data points at a starting point of (θ_1^i, ϕ_1^i).

2) Remove offset drifts by fitting with polynomial of degree 3.

3) Wavelet Analysis : $B_{21x} \rightarrow B_{21x}^{wt}$

Set the wavelet coefficients which are at level 7 or above to be zero. Perform an inverse transformation to get B_{21x}^{wt}.

4) For the 600 data points, get rms average of B_{21x}^{wt}:

$$B_{21x,rms} = \sqrt{\sum_i (B_{21x}^{wt}(t))^2/600}\,. \qquad (10)$$

5) Get rms average of 10 windows :

$$\langle B_{21x,rms}\rangle = \sqrt{\sum_{k=1}^{N}{}'(B_{21x,rms}(k))^2/N},\ N \le 10 \qquad (11)$$

The prime in Σ' means that the windows which satisfy

$$B_{21x,rms}(k) > rmspar \qquad (12)$$

are removed in the summation. The *rmspar* is a constant which is determined by experience.

6) Find (θ_1^f, ϕ_1^f) which minimizes $< B_{21x,rms} >$.

The directions of y_2 and z_2 axes, (θ_2^f, ϕ_2^f) and (θ_3^f, ϕ_3^f) can be determined likewise.

3. Results and Discussion

The data used in this analysis were taken at 1 Hz using 3 fluxgate sensors which were placed on a line at the sea bottom about 50 m under the sea surface. The distance between adjacent sensors was 100 m and the sensor axes were not aligned. The data were measured for about 22 hours. As described in section 2, the data were divided into windows which consist of 600 data points each.

Fig. 4 shows the data and preprocessed results of two windows between 840 and 860 minutes. Fig. 4(a), (b), and (c) show the x, y, and z components of magnetic fields for sensor 1 and sensor 2, respectively. Because the daily change of the geomagnetic field is large and offset drift of each sensor axis is also significant, the minimum of each window was set to zero in the figures so that only

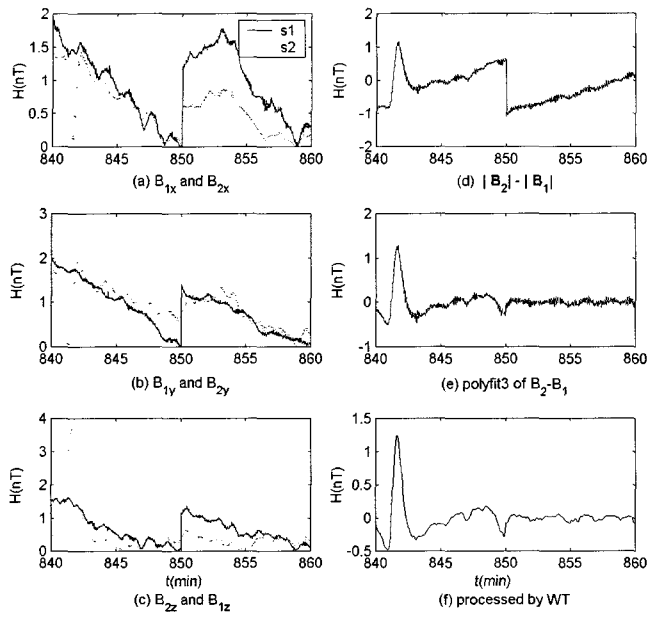

Fig. 4. (a) x, (b) y, and (c) z components of magnetic fields measured by two sensors S1 and S2. (d) $|\boldsymbol{B}_2| - |\boldsymbol{B}_1|$, (e) processed data by polynomial (order 3) fitting, (f) results by wavelet analysis in which wavelets of level 7 or higher ones were removed.

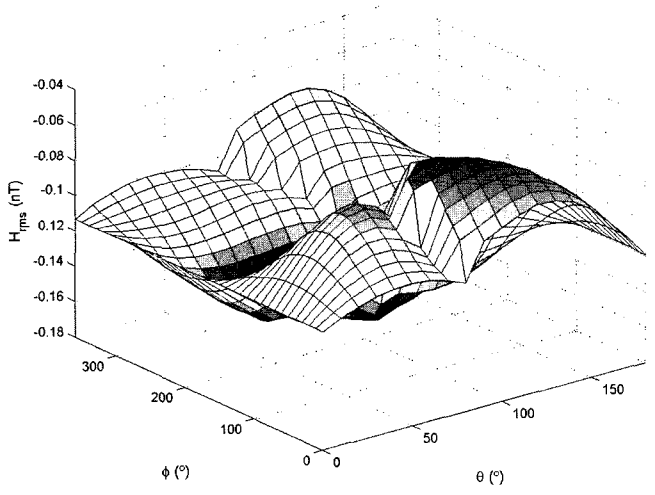

Fig. 5. Averaged rms noise of geomagnetic field, $-\langle B_{21x,\,rms}\rangle$ with rmspar = 0.20 as a function of θ_1 and φ_1 of x' axis.

short time changes of geomagnetic field can be seen.

In Fig. 4(d), the result obtained by applying subtraction filter to the absolute values of $\boldsymbol{B}_1$ and $\boldsymbol{B}_2$ is shown. The curve fit result of Fig. 4(d) with a polynomial of order 3 is shown in (e). In Fig. 4(f), the processed data after wavelet transformation is shown. In this figure, we can see that noises with frequencies higher than 100 mHz have been completely removed. In the window between 840 and 850 min, a target signal is observed on sensor 2 which shows the effect indicated by equation (4). From Fig. 4(a), (b), and (c) the peak height of the target signal is expected to be larger than 3 nT, but it is only 1.7 nT in Fig. 4(f), which is the evidence of the term $(\boldsymbol{R}/R)\cdot\boldsymbol{b}$.

Table 1. The angles of detection sensor axes in degrees in the coordinate system of the reference sensor. In the notation of S*ij*, *i* denotes the reference sensor and *j* denotes the detection sensor.

	(θ_1, ϕ_1)	(θ_2, ϕ_2)	(θ_3, ϕ_3)
S12	(83.2, 68.0)	(97.0, 159.7)	(11.6, -155.0)
S23	(88.5, -115.7)	(98.3, -26.2)	(7.9, -6.5)
S13	(85.3, -47.2)	(87.7, 41.8)	(6.6, 163.5)

Fig. 5 shows average rms noise of B_{21x}, $\langle B_{21x,rms}\rangle$ in equation (11) as a function of θ_1 and ϕ_1, where x_1' axis in Fig. 2 is not aligned to x_2 axis and has an arbitrary direction (θ_1, ϕ_1). In order to see the minima clearly $-\langle B_{21x,rms}\rangle$, was plotted rather than $\langle B_{21x,rms}\rangle$. From Fig. 5, we see that $\langle B_{21x,rms}\rangle$ has more than one local minimum.

In applying the algorithm in section 2.2.3, eight different starting points, one in each octant, were used for the minimization process. Then the program reaches two or three local minima and the lowest one was chosen as the desired minimum. Among the minimization algorithms, the Nelder-Mead simplex method [3] gave the most reliable results though it is relatively slow. For values of *rmspar* in equation (12), 0.2 or 0.25 nT yields good results.

Table 1 shows the results of the minimization process. The angles of detection sensor with respect to the coordinate system of the reference sensor are listed. In the notation of a sensor pair S*ij*, *i* denotes the reference sensor and *j* denotes the detection sensor : (θ_1, ϕ_1), (θ_2, ϕ_2) and $(\theta_3, \phi_3)$of S12 denotes the angles of x, y, and z axes of sensor 2 with respect to sensor 1's coordinate axes. The errors in the angles were estimated by performing the procedure in several different time ranges. The estimated error range is ±2° except ±5° for ϕ_3 of S13. The large error in ϕ_3 of S13 indicates that θ_3 of z axis of sensor 3 is so small that the determination of ϕ_3 may not be accurate.

The reliability of the estimated angles were tested in the following way. The rotation matrix $\boldsymbol{A}_{ij}$ in equation (6) was calculated by equation (7) for S12, S13, and S23. If we calculate $\boldsymbol{A}'_{13}=\boldsymbol{A}_{12}\boldsymbol{A}_{23}$, then $\boldsymbol{A}'_{13}$ must be the same as $\boldsymbol{A}_{13}$. We verified that $\boldsymbol{A}'_{13} \approx \boldsymbol{A}_{13}$ within an error limit. As another verification, the angles of sensor 3's axes were calculated from the matrix elements of $\boldsymbol{A}'_{13}$, which gives two ϕ's for each axis. The results are shown in Table 2. The coincidence is remarkable except for ϕ_3, where a large error in ϕ_3 is expected due to small θ_3 as discussed above.

The coherence of two signals is defined by [1, 2]

Table 2. Angles of sensor 3's axes with respect to sensor 1, which were calculated from the elements of A'_{13}, were compared with the results of S13 in Table 1.

	(θ_1, ϕ_1)	(θ_2, ϕ_2)	(θ_3, ϕ_3)
S13	(85.3, -47.2)	(87.7, 41.8)	(6.6, 163.5)
A'_{13}	θ'_1=85.2 ϕ'_1=-47.5 -45.5	θ'_2=89.0 ϕ'_2=40.3 42.9	θ'_3=8.7 ϕ'_3=139.2 165.8

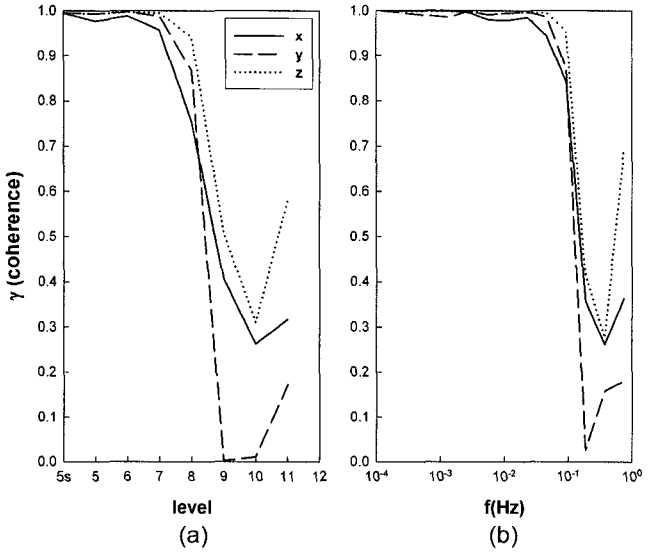

Fig. 6. Coherence of (a) WT, and (b) FT coefficients.

$$\gamma = \sqrt{\frac{|F_d^* F_r|^2}{|F_d|^2 |F_r|^2}} \tag{13}$$

where F_d and F_r are Fourier (or wavelet) coefficients of detection and reference signals, respectively. The coherence of B_{2x} and B'_{1x} in equation (8) and the corresponding coherences of y and z components are shown in Fig. 6. The coherences of wavelet coefficients are shown in Fig. 6(a) and those of Fourier coefficients are shown in Fig. 6(b). In Fig. 6(a), 5s on the abscissa denotes the scaling function at level 5 and the other numbers denote the levels of wavelets (refer to Fig. 3 for the frequency range of each level). The coherences of Fourier coefficients were calculated by constant Q averaging. The Fourier coefficient of three components of $\boldsymbol{B}_2$ and $\boldsymbol{B}'_1$ show $\gamma > 0.97$ in a frequency range of 0~30 mHz and the wavelet coefficients show $\gamma > 0.97$ up to level 6 wavelets. For some ranges of time and for certain components of magnetic field, the detection and reference signals show very good coherences of better than 0.99 if there is no target signal in the window.

Once we obtain the directions of detection sensor axes with respect to reference sensor, we can process the three components of magnetic fields separately by subtraction filter, polynomial fitting, and wavelet transformation successively. Thereafter, we can get absolute values of magnetic fields. In this processing, polynomial of order 2 was used because fitting with polynomial of order 3 may reduce the target signal. For processing data with wavelet transformation, the same procedure in section 2.2.3 was used. In Fig. 7, the data obtained with this method are compared with the data which are processed as in Fig. 4(f), where absolute values of $\boldsymbol{B}$'s are first calculated followed by subtraction filtering, polynomial fitting, and wavelet processing. The rms noise of the geomagnetic signal for 1,000 s data starting from 3.5 hour was reduced by 9.1 dB compared with the latter method. The noise can be reduced further by applying other wavelet processing techniques [4, 5].

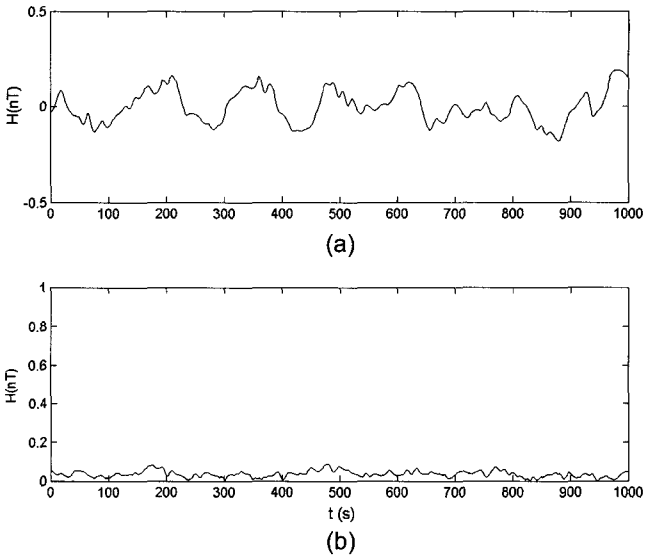

Fig. 7. Final results by two different processing methods : (a) B_2-B_1, (b) rotation of axes.

4. Conclusion

Noise reduction of geomagnetic signals using subtraction filtering was discussed. If axis directions of two flux-gate sensors are not aligned, the absolute values of the observed magnetic field lose good coherence between them even in the low frequency range due to the offset drift vectors of both sensors which have unknown directions and magnitudes. Therefore, applying subtraction filter to the absolute values of the magnetic field does not give good results.

A method of finding the axis directions of the second sensor with respect to the first one was presented and validity of this method was also discussed. The components

of magnetic field of a detection sensor can be processed applying subtraction filtering with the corresponding components which are calculated by rotating the axes of the reference sensor. Applying polynomial fitting to the results from subtraction filtering makes it possible to remove the offset drifts of the two sensors. Further noise reduction can be achieved by processing the data with wavelet transformation.

References

[1] Brooks C. Fowler, H. W. Smith, and F. X. Bostic, Jr., "Magnetic Anomaly Detection Utilizing Component Differencing Techniques", Report for the Office of Naval Research, p. 25 (1973).

[2] E. J. Eidem, "Measurements and Analysis of Fluctuations in the Earths Magnetic Field in a Coastal Water Area", MARELEC, **197**, Proc. S5 (1997).

[3] W. H. Press, et al., "Numerical Recipes in Fortran 77", Cambridge University Press, p. 402 (1996).

[4] D. Donoho, "Nonlinear Wavelet Methods for Recovery of Signals, Densities, and Spectra from Indirect and Noisy Data", Proc. Sym. Appl. Math., p. 173 (1993).

[5] Quinquis and S. Rossignol, "Noise Reduction, with a Noise Reference, of Underwater Magnetic Signals", Digital Signal Proc., **6**, pp. 240-248 (1996).